Isomers and hindrances in ^{254}No: A touchstone for theories of superheavy nuclei

S. G. Wahid,[1,*] P. Chowdhury,[1,†] D. Seweryniak,[2] T. L. Khoo,[2] F. G. Kondev,[2] R. M. Clark,[3] B. B. Back,[2,‡] P. C. Bender,[1] M. P. Carpenter,[2] P. A. Copp,[2] K. Hauschild,[4] G. Henning,[5] R.-D. Herzberg,[6] D. E. M. Hoff,[1,§] T. Huang,[7,2] H. Jayatissa,[2] A. Korichi,[8] T. Lauritsen,[2] A. Lopez-Martens,[4] G. Morgan,[9] C. Morse,[3,‖] C. Müller-Gatermann,[2] D. H. Potterveld,[2] W. Reviol,[2] A. M. Rogers,[1] S. Saha,[1] G. Savard,[2] K. Sharma,[1] S. Waniganeththi,[1] G. L. Wilson,[2] J. Wu,[2,‖] and S. Zhu[10,‡]

[1]*Department of Physics, University of Massachusetts Lowell, Lowell, Massachusetts 01854, USA*
[2]*Physics Division, Argonne National Laboratory, Argonne, Illinois 60439, USA*
[3]*Nuclear Science Division, Lawrence Berkeley National Laboratory, Berkeley, California 94720, USA*
[4]*IJClab, Université Paris Saclay, CNRS, F-91405 Orsay, France*
[5]*Université de Strasbourg, CNRS, IPHC/DRS UMR 7178, 23 Rue du Loess, F-67037 Strasbourg, France*
[6]*University of Liverpool, Liverpool L697ZE, United Kingdom*
[7]*Institute of Modern Physics, Chinese Academy of Sciences, Lanzhou 730000, China*
[8]*CNRS/IN2P3, IJCLab, 91405 Orsay Campus, France*
[9]*Louisiana State University, Baton Rouge, Louisiana 70803, USA*
[10]*National Nuclear Data Center, Brookhaven National Laboratory, Upton, New York 11973, USA*

(Received 13 October 2024; revised 20 January 2025; accepted 26 February 2025; published 13 March 2025)

We report on a new spectroscopic study of the decay of high-K isomers in $^{254}_{102}No_{152}$, a touchstone nucleus for testing models to understand the structure of superheavy nuclei. The experiment, performed using the Argonne gas-filled analyzer (AGFA), was geared toward resolving long-standing ambiguities in spin-parity and configuration assignments for the two- and four-quasiparticle (qp) intrinsic excitations identified in this nucleus. The isomer decay schemes are firmly established with the help of the highest-statistics γ-γ coincidence data collected to date, providing anchor points for competing theories. A newly measured half-life in the nanosecond range establishes a second 2-qp isomer in ^{254}No. The preferred decay pathways for the 2- and 4-qp isomers are discussed, providing new insights into the underlying hindrance mechanisms at play in these heavy nuclei. With firm configuration assignments, the intrinsic excitations in this deformed mass region provide stringent constraints and challenge the different theoretical approaches at play in understanding the structure of superheavy nuclei.

DOI: 10.1103/PhysRevC.111.034320

I. INTRODUCTION

The study of superheavy elements is a frontier area of current research in nuclear physics. Theories that attempt to predict the properties of shell-stabilized superheavy nuclei (SHN) rely on a knowledge of the single-particle energy (SPE) spectrum. Detailed information in this regard stems mostly from spectroscopic studies of deformed nuclei in the $Z \gtrsim 100$ region [1,2], originating from the discovery that quantal shell effects allow heavy deformed nuclei like ^{254}No ($Z = 102$, $N = 152$) to survive fission and sustain angular momenta beyond $20\hbar$ [1,3]. While elements up to $Z = 118$ have been synthesized by fusion reactions [4], production cross sections that allow detailed spectroscopic investigation are limited to nuclei in the $Z \gtrsim 100$ region. Nuclei in this region are axially deformed, with valence orbitals that may originate from above the spherical superheavy shell gaps. In addition to collective rotational states with fast decays, these nuclei also exhibit long-lived excitations (isomers) from intrinsic couplings of valence nucleons, which reflect underlying symmetries in their wave functions. Axially deformed nuclei exhibit isomers whose decays are hindered by K-selection rules, where K is the projection of the total angular momentum on the symmetry axis. Establishing the energies, spins and configurations of K-isomers in the deformed $Z \gtrsim 100$ nuclei, therefore, provides a test of SPEs in spherical superheavy nuclei.

The unexpectedly large shell effects in these deformed nuclei have also spurred considerable theoretical activity to reproduce the single-particle energies and gaps and have ushered in new physics ingredients such as the need to include higher order deformations that minimize mass and increase

*Contact author: sgwahid@gmail.com
†Contact author: partha_chowdhury@uml.edu
‡Deceased.
§Present address: Nuclear and Chemical Sciences Division, Lawrence Livermore National Laboratory, Livermore, California 94550, USA.
‖Present address: National Nuclear Data Center, Brookhaven National Laboratory, Upton, New York 11973, USA.

stability [5]. The presence of sub-shell gaps is also manifested in the excitation energies of 2- and 4-qp K-isomers in nuclei around these gaps. Macroscopic-microscopic (MM) theories predict the observed sub-shell gaps for protons at $Z = 100$ and neutrons at $N = 152$ [6], while purely microscopic self-consistent theories predict gaps at various proton and neutron numbers, e.g. $Z = 98$ and $N = 150$, depending on the specific choice of interactions [7]. The ^{254}No isomers represent a best-case experimental scenario for testing the current theoretical landscape, as they are populated with relatively large cross sections, together with the fact that an array of theoretical calculations is presently available in this region, and more specifically, for this "pioneer" nucleus. Configuration-constrained potential energy surface calculations [8,9] using an axially-symmetric Woods-Saxon potential with a universal parameter set (including β_6 deformation) for 2- and 4-quasiparticle (qp) configurations in ^{254}No and neighboring nuclei are very different from predictions of density functional theories [10–12]. A consistent framework for each such theoretical approach needs to be well validated in this mass region before they can be extrapolated to the spherical superheavy nuclei.

The present work reports on a new spectroscopic study of the decay of high-K isomers in $^{254}_{102}$No$_{152}$, performed at Argonne National Laboratory using a new gas-filled analyzer to separate beam and reaction products. Prior work on ^{254}No from four different groups around the world had established a 2-qp and a 4-qp K-isomer, [13–16]. However, these studies lacked consensus on the excitation energy, spin-parity, and decay pathways of the higher-lying 4-qp isomer, as well as the configuration of the 2-qp $K^\pi = 8^-$ isomer. The isomer decay schemes are firmly established in the present work with the highest γ-γ coincidence dataset on this nucleus collected to date. A new short half-life in the nanosecond region, measured using the centroid-shift method, establishes a second 2-qp isomer in ^{254}No, expanding the discussion of nucleon orbitals involved in the multi-qp excitations.

II. EXPERIMENT AND DATA ANALYSIS

Excited states in ^{254}No were populated using the ^{208}Pb(^{48}Ca, 2n)^{254}No fusion evaporation reaction. The ^{48}Ca beam with an average energy of 218 MeV (center of the target) and an average intensity of ≈200 pnA was provided by the ATLAS linear accelerator at Argonne National Laboratory. Sixteen isotopically enriched (≈99%) ^{208}Pb target segments with ≈0.5 mg/cm^2 thickness were mounted on a rotating wheel to minimize target degradation. A 40 (10) μg/cm^2 thick carbon layer covered the front (back) of the targets, to avoid sputtering and allow better cooling as well as to cover any pinholes in the targets. Periodic beam sweeping was set up to avoid the beam hitting the target wheel spokes, and horizontal wobbling at ≈5 Hz frequency was used to spread the beam over a larger target area. The ^{254}No evaporation residues were transported through the Argonne Gas Filled Analyzer (AGFA), which utilizes a novel large-bore vertical-focusing quadrupole magnet and a combined-function horizontal-focusing dipole magnet to separate the residues from the unreacted beam and other unwanted reaction products. The helium gas pressure was 0.49 Torr, and a magnetic rigidity ($B\rho$) of 2.14 Tm optimized the transport of ^{254}No nuclei. A parallel-grid avalanche counter (PGAC), located at the exit from AGFA, served as a tag for the recoils implanted in a 300-μm-thick 64 × 64 mm^2 double-sided Si strip detector (DSSD) with 160 × 160 = 25 600 pixels at the AGFA focal plane. The implant detector was surrounded by an array of eight 4 × 7 cm^2 300-μm-thick single-sided Si strip detectors in a tunnel-box geometry to detect escaping decay particles. A 5 × 5 cm^2 300-μm-thick Si detector was placed behind the DSSD to veto energetic light particles, e.g., protons and α particles, which passed undetected through the PGAC. The focal plane Si detectors were surrounded by the X-array, consisting of a simple box-like geometry of five HPGe clover detectors with ≈65% solid angle coverage of 4π and a total photopeak efficiency of ≈10% at 1.3 MeV [17]. Isomeric decays were identified by time and spatial correlations, i.e., the detection of an electron signal within a specified decay time (optimized for the isomer half-life) in the same pixel where an evaporation residue was implanted. The decay of a K-isomer in deformed SHN in this region, in general, populates a rotational band with highly converted low-energy transitions. These are predominantly conversion electrons (CE), and the implant pixel in the DSSD works as a calorimeter for the CEs, Auger electrons, as well as L and M x-rays. The X-array was used to record γ rays in coincidence with decay events in the DSSD. The raw data were sorted into appropriate energy and time histograms and analyzed using the ROOT [18] and RADWARE [19] suites of programs. To isolate events from different isomeric states, time conditions were employed on the decay electrons in the DSSD with respect to the recoil signals in PGAC, and γ transitions correlated in time with the decay electrons in the DSSD pixels inspected. Histograms of the time difference between recoil implant events and decay electrons as well as γ transitions and decay electrons were analyzed to extract half-lives in various time ranges.

To measure half-lives in the nanosecond range, an electron-energy-dependent "walk" in the time response of the DSSD was corrected event-by-event using the signal waveforms collected during the experiment. Each correlated decay trace was fitted with a linear background and a parabolic rise to accurately determine the pulse start. Since waveform traces were not recorded for the γ rays in the clover detectors, data from a ^{152}Eu source was used to quantify their energy-dependent time walk by inspecting γ-γ time differences as a function of γ-ray energy. A time walk of <0.5 ns is inferred for $E_\gamma > 500$ keV in the clovers with an overall time-walk uncertainty between the DSSD and clover detectors of below a nanosecond. This analysis was critical for deducing a reliable half-life in the nanosecond range for the new isomer using the centroid shift method.

III. EXPERIMENTAL RESULTS

The isomer decay scheme of ^{254}No established in the present experiment is shown in Fig. 1. The two previously observed K-isomers in this nucleus are corroborated here, and their half-lives remeasured. The CE time distributions, correlated with the ^{254}No recoils, clearly show two distinct

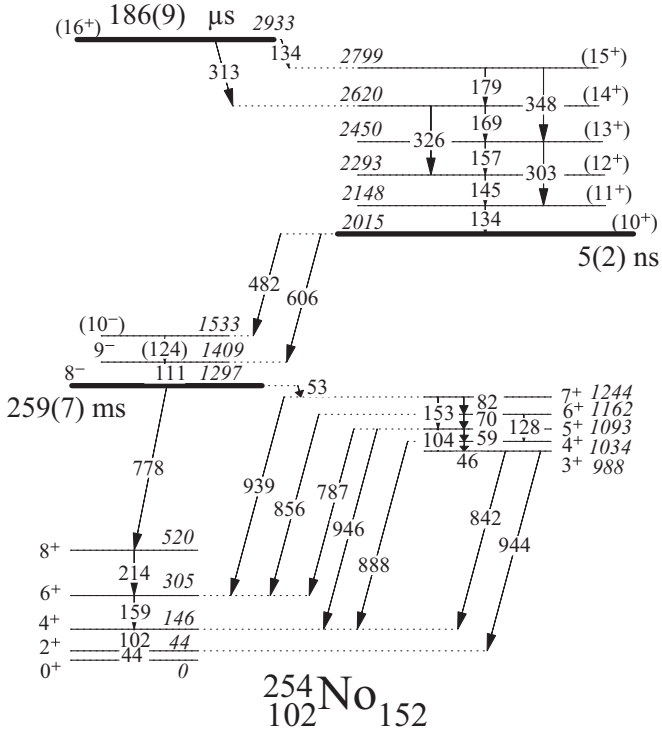

FIG. 1. Partial decay scheme of ^{254}No established from the present work. The half-life of the $K^\pi = 10^+$ at $E_x = 2015$ keV is newly determined while those of the $K^\pi = 8^-$ and $K^\pi = 16^+$ are in agreement with prior work [13–16].

decay behaviors and had been utilized in the previous studies to deduce the half-lives. However, significant statistics for the strongest γ transitions in the decays, viz., 606-keV from the 4-qp and 944-keV from the 2-qp isomers, enabled a direct look at the time distribution of these γ rays instead. Figure 2 shows the decay curves, with extracted half-lives of 259(7) ms for the 2-qp isomer and 186(9) μs for the 4-qp isomer, in very good agreement with earlier measurements [13–16]. The 1297-keV excitation energy of the lower-lying isomer is also consistent with all previous measurements. The higher-lying isomer is placed at an excitation energy of 2933 keV, which agrees within uncertainties with the work of Clark *et al.* [15], with all states and γ rays placed in their earlier level scheme corroborated here.

Relevant information related to transitions assigned to the decay of the 4-qp and 2-qp isomers are listed in Tables I and II, respectively. While there is consensus on both the level energy and spin-parity assignment of $K^\pi = 8^-$ for the lower

TABLE I. Energies (E_γ) and intensities (I_γ) of γ rays (relative to the 606-keV transition), excitation energies (E_i, E_f), the total intensity ($I_{\rm tot}$) corrected for internal conversion using pure transition multipolarities, and assigned spin-parities (I_i^π, I_f^π) of initial and final states using intensity balance, for the decay of 4-qp isomer in ^{254}No. Transition energies are accurate to within 0.5 keV and statistical uncertainties on γ-ray intensities are listed.

E_γ(keV)	E_i(keV) → E_f(keV)	$I_i^\pi \to I_f^\pi$	I_γ	$I_{\rm tot}$
111.4	1409 → 1297	$9^- \to 8^-$	10.5(9)	111(10)
(124)	1533 → 1409	$(10^-) \to 9^-$		
133.5[a]	2148 → 2015	$(11^+) \to (10^+)$	15.1(9)[a]	100(6)
133.5[a]	2933 → 2799	$(16^+) \to (15^+)$	13.6(8)[a]	90(5)
145	2293 → 2148	$(12^+) \to (11^+)$	17.1(15)	93(8)
157.3	2450 → 2293	$(13^+) \to (12^+)$	5.2(6)	84(9)[b]
169.3	2620 → 2450	$(14^+) \to (13^+)$	5.5(6)	74(7)[b]
179.4	2799 → 2620	$(15^+) \to (14^+)$	6.7(6)	78(7)[b]
302.9	2450 → 2148	$(13^+) \to (11^+)$	1.5(4)	2.0(5)
313.4	2933 → 2620	$(16^+) \to (14^+)$	4.2(5)	5.5(7)
325.9	2620 → 2293	$(14^+) \to (12^+)$	3.6(5)	4.6(6)
348.2	2799 → 2450	$(15^+) \to (13^+)$	4.4(6)	5.4(7)
481.6	2015 → 1533	$(10^+) \to (10^-)$	4.1(6)	4.1(6)
605.8	2015 → 1409	$(10^+) \to 9^-$	100.0(27)	101.3(27)

[a]134-keV doublet.
[b]For mixed $M1/E2$ analysis for these transitions, see text.

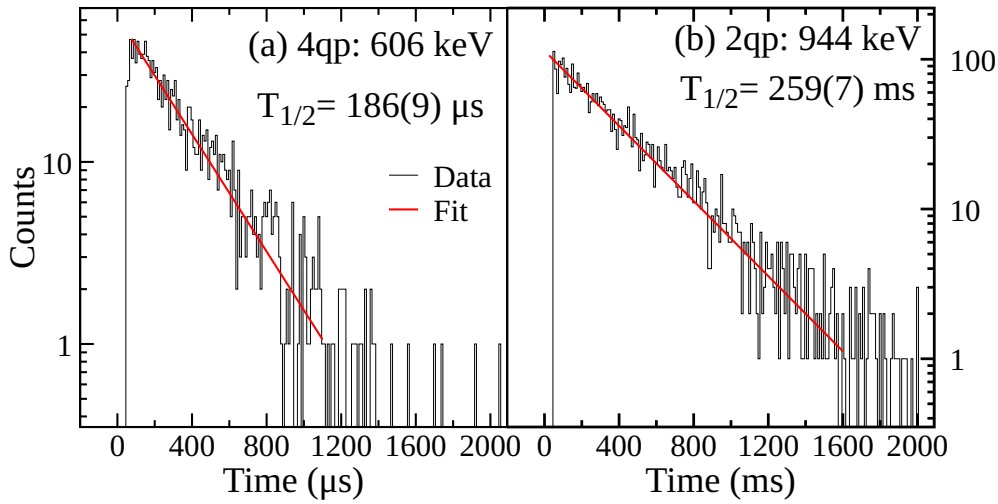

FIG. 2. Spectra of time difference between recoil implants and (a) the 606-keV γ rays from the 4-qp, $K^\pi = 16^+$ isomeric decay and (b) 944-keV γ rays decaying from 2-qp, $K^\pi = 8^-$ isomeric state in ^{254}No. Only statistical uncertainties are quoted in the fitted half-lives.

TABLE II. Energies (E_γ) and intensities (I_γ) of γ rays (relative to the 944-keV transition), excitation energies (E_i, E_f), the total intensity ($I_{\rm tot}$) corrected for internal conversion using pure transition multipolarities and assigned spin-parities (I_i^π, I_f^π) of initial and final states using intensity balance for the decay of the $T_{1/2} = 259(7)$ ms 2-qp isomer in ^{254}No at $E_x = 1297$ keV. Transition energies are accurate to within 0.5 keV and statistical uncertainties on γ-ray intensities are listed.

E_γ(keV)	E_i(keV) $\rightarrow$ E_f(keV)	$I_i^\pi \rightarrow I_f^\pi$	I_γ	$I_{\rm tot}$
53.4	1297 $\rightarrow$ 1244	$8^- \rightarrow 7^+$	23.3(5)	42(1)
69.6	1162 $\rightarrow$ 1093	$6^+ \rightarrow 5^+$	1.1(1)	48(5)
82.1	1244 $\rightarrow$ 1162	$7^+ \rightarrow 6^+$	1.9(1)	50(4)
102[a]	146 $\rightarrow$ 44	$4^+ \rightarrow 2^+$	2.4(2)[a]	
128[b]	1162 $\rightarrow$ 1034	$6^+ \rightarrow 4^+$	0.5(2)	6(2)
152.8	1244 $\rightarrow$ 1093	$7^+ \rightarrow 5^+$	2.2(2)	13(1)
159.1	305 $\rightarrow$ 146	$6^+ \rightarrow 4^+$	1.7(1)	9(1)
214.2	520 $\rightarrow$ 305	$8^+ \rightarrow 6^+$	1.5(1)	3.3(3)
778.4	1297 $\rightarrow$ 520	$8^- \rightarrow 8^+$	3.6(3)	3.6(3)
787.2	1093 $\rightarrow$ 305	$5^+ \rightarrow 6^+$	2.1(3)	2.5(3)
841.6	988 $\rightarrow$ 146	$3^+ \rightarrow 4^+$	37(1)	42(1)
856.4	1162 $\rightarrow$ 305	$6^+ \rightarrow 6^+$	3.0(3)	3.4(3)
887.7	1034 $\rightarrow$ 146	$4^+ \rightarrow 4^+$	9.5(5)	10(1)
939.1	1244 $\rightarrow$ 305	$7^+ \rightarrow 6^+$	4.5(6)	5.0(4)
943.9	988 $\rightarrow$ 44	$3^+ \rightarrow 2^+$	100(2)	111(2)
946.3	1093 $\rightarrow$ 146	$5^+ \rightarrow 4^+$	2(1)	2(1)

[a]102- and 104-keV doublet.
[b]Extracted from excess of 128 in the K_{β_2}.

isomer in all prior work, the case for the upper isomer has not been so clear-cut. Since that was the primary motivation for the present work, the decay of the 4-qp isomer is discussed first. The placement of the most prominent 606-keV γ transition in its decay pathway has been debated. It was observed earlier in in-beam data, ruling it out as a direct decay transition from the 4-qp isomer [20,21]. Whether the decay of the isomer proceeds through a single rotational band built on the 2-qp $K^\pi = 8^-$ isomer [13,14,16] or through two, via an intermediate $K^\pi = 10^+$ rotational band [15], was not definitive. Although the latest work included some γ-γ coincidence data, the scant statistics of just a few counts in these spectra needed improvement.

The rotational band nestled in the decay pathway of the higher isomer to the lower isomer is now anchored with confidence on the basis of improved γ-γ coincidence statistics. The bandhead also exhibits a half-life in the nanosecond range, measured in the present work using centroid shift techniques described below. The new information allows a more informed discussion of configuration assignments in this nucleus, which are critical for understanding the evolving nuclear structure in this region but are still under debate.

The placements of the previously reported γ rays and level energies above the 2-qp, $E_x = 1297$ keV, $K^\pi = 8^-$ isomer as reported in Ref. [15] have now been verified and expanded, based on observed γ rays, both in singles and in their coincidence relationships in two-dimensional energy-energy histograms. The γ-ray spectra observed in the decay of the 4-qp isomer are shown in Fig. 3(a). Each of the four germanium crystals within a clover detector is considered here as a standalone detector. This maximizes detector granularity for γ-γ coincidences and minimizes the summing effect of two distinct γ events in neighboring clover crystals. The 482-keV γ ray, first reported by Clark *et al.* [15], is observed and placed with confidence in the decay scheme (Fig. 1) based on coincidence relations. The present data unambiguously confirm that the 606-keV γ ray is in coincidence with the 111-, 134-, 145-, 157-, 169-, 179-, 313-, 326- and 348-keV γ rays reported earlier in the decay of 4-qp isomer. It is not in coincidence, however, with the 482-keV γ ray [Fig. 3(b)]. Based on the total intensity of the 482-keV γ ray in the singles spectrum, at least eight counts were expected in the 606-keV gate if in coincidence (similar to the 326-keV peak), but none were observed.

As noted earlier, the positioning of the 606-keV transition in the decay sequence, the strongest from the 4-qp isomer decay, has also been a subject of debate. Some earlier studies [13,14,16] suggested it to be decaying from states close to the upper 4-qp isomer and feeding a single rotational band built on the lower 2-qp isomer. It was first placed in its current position in the level scheme in Ref. [15] as a direct decay from the $E_x = 2015$ keV, $K^\pi = 10^+$ state. The present data are in agreement with this placement. This is additionally substantiated by the fact that the 606-keV γ ray is observed in the present work to exhibit a delay with respect to the CEs from the 4-qp isomer decay through the rotational band structure. Figure 4 shows the time difference between 606-keV γ rays and their coincident CEs compared to a "prompt" reference combination consisting of 944-keV γ rays and their coincident CEs in the decay of the 2-qp isomer. A distinct shift in the centroid is observed. As a cross-check, a second combination consisting of 842-keV γ rays and their coincident CEs in the decay of the 2-qp isomer show the same shift within $<$1 ns. Details of the careful analysis for extracting these time-difference spectra after correcting for energy-dependent time walks for both electrons and γ rays have been described earlier, where the uncertainties due to walk in both CEs and clovers are $<$1 ns. The magnitude of the shift implies a half-life $T_{1/2} = 5(2)$ ns and is assigned to the $K^\pi = 10^+$ state at $E_x = 2015$ keV. The conservative uncertainty quoted reflects the 10 ns granularity of the time clock in the data acquisition. The identification of a measurable half-life of the 2015-keV state provides additional support for its placement as the head of a rotational band that is distinct from one built on the 1297-keV, $K^\pi = 8^-$ isomer.

The doublet character of the 134-keV γ ray reported in Ref. [15] is also confirmed from its self-coincidence in the 134-keV γ-gated spectrum shown in Fig. 3(c). The 313-keV γ ray was observed in prior studies [15,16], though placed only in the decay scheme in Ref. [15]. In addition, a new 303-keV γ ray is observed in singles [Fig. 3(a)] as well as in coincidence with the 606-keV γ ray [Fig. 3(b)]. The 303-keV γ ray is assigned as a crossover $E2$ transition decaying from the $E_x = 2450$-keV state (Fig. 1) because it satisfies the energy sum of two consecutive $M1$ transitions in the rotational band.

The decay of the 2-qp, $K^\pi = 8^-$ isomeric state yields many prominent γ rays, mainly in the range 40 keV $< E_\gamma <$

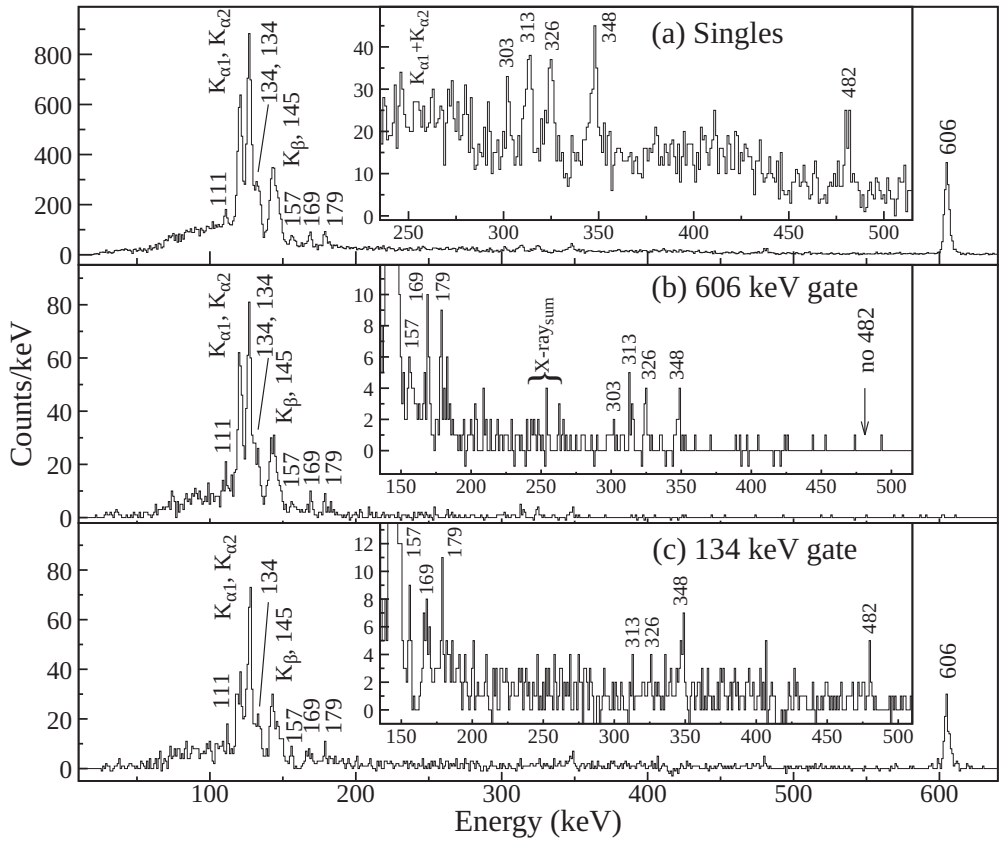

FIG. 3. (a) Singles γ-ray spectrum in prompt coincidence with delayed conversion electron (CE) bursts from the 4-qp, $K^\pi = 16^+$, isomer decay following a recoil implant in the same DSSD pixel; (b), (c) CE-gated γ-ray spectra in coincidence with the 606- and 134-keV transitions, respectively.

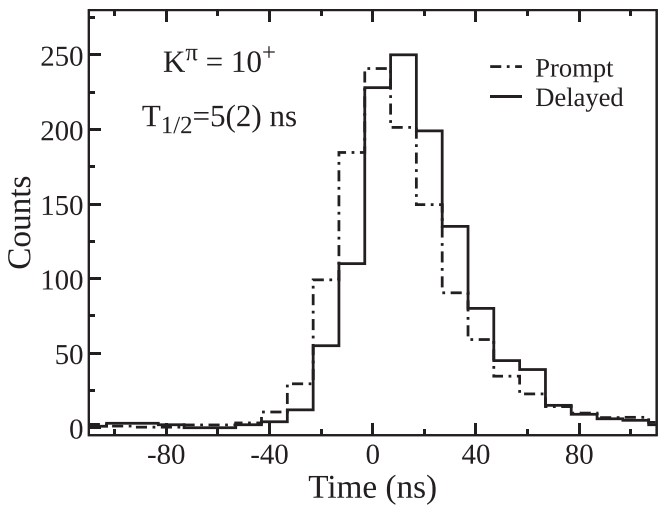

FIG. 4. Half-life measurement using the centroid-shift technique: $T_{1/2} = 5(2)$ ns for the $K^\pi = 10^+$ state in ^{254}No. The solid curve is the time difference between 606-keV γ rays deexciting the 10^+ state and CEs feeding it from the decay of the upper 4-qp isomer, while the dotted one is the time difference between the 944-keV γ ray in "prompt" coincidence with CEs from the decay of the lower 8^- isomer (see text).

250 keV and 700 keV $< E_\gamma <$ 1000 keV, with no significant peaks in between [Fig. 5(a)]. As proposed previously, the decay proceeds through two branches, a 778-keV direct γ decay to the 8^+ member of the ground state band, and a 53-keV transition populating the 7^+ member of a rotational band built on the 988-keV 3^+ state. This work provides direct γ-γ coincidence evidence for these placements. Figures 5(d) and 5(e) clearly show that the 778 keV transition is not in coincidence with the 53-keV but is in coincidence with 102-, 159- and 214-keV transitions in the ground state rotational band, substantiating its placement in the level scheme as a $\Delta K = 8$, $E1$ transition. In addition, the $E1$ multipolarity determination of the 53-keV transition in this work described below corroborates the parity change in decaying from the 8^- isomer to the 7^+ member of the 3^+ band.

A few new weak peaks are observed in singles that could constitute additional connections between states built on the 3^+ band and the 8^- isomer, such as the 135-, 205- and 216-keV transitions. These are not placed in the current level scheme because they could not be confirmed with the low-statistics coincidence data.

Multipolarity assignments for transitions with sufficient statistics are based on intensity balances, as well as arguments based on parallel branches and crossover transitions. The strongly coupled rotational band structure built on the

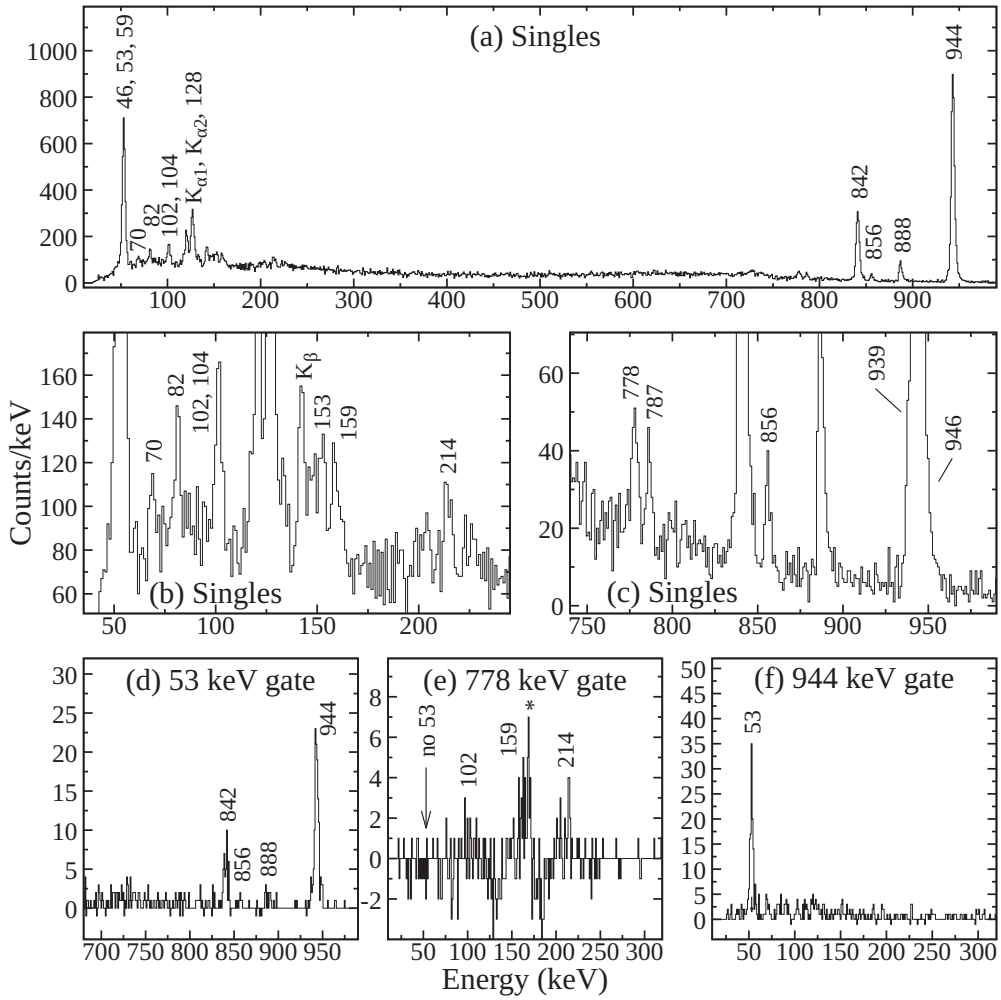

FIG. 5. (a) Singles γ-ray spectrum in prompt coincidence with delayed CE bursts from the 2-qp 8^- isomer decay following a recoil implant in the same DSSD pixel; (b), (c) expanded regions of panel (a) showing weak transitions; (d)–(f) CE-gated spectra from the decay of the 2-qp 8^- isomer, gated on specific gamma-ray transitions. The asterisk in panel (e) is a 166-keV Compton scatter of the strong 944-keV γ ray that appears in the 778-keV gate due to the close geometry of the Ge clover crystals.

2015-keV state follows the expected $M1$ and $E2$ intensity pattern. Intensity balance arguments are especially useful for low-energy transitions where conversion coefficients [22] are quite distinct for the low multipolarities, such as the 134-keV γ ray out of the 4-qp isomer, the 111-keV transition in the rotational band built on the 8^- isomer, and the 53-keV γ ray out of the 2-qp, $K^\pi = 8^-$ isomer. For these transitions, an extracted conversion coefficient from imposing intensity balance is compared to possible multipolarities (Fig. 6), showing the validity for their assignments.

The spin-parity assignment of the 2-qp $K^\pi = 8^-$ isomeric state is now well established and agreed upon from all experiments to date. The next intrinsic state (or bandhead) at 2015 keV, with a now-measured half-life of 5(2) ns, decays via two parallel transitions with an energy difference of 124 keV, with the stronger 606-keV transition observed to be coincident with a 111-keV $M1$ transition [Fig. 3(b)]. Two consecutive transitions with energies of 111 keV and 124 keV (albeit unresolved due to its weak population via the 482-keV transition as well as being swamped by nobelium K_α x-rays), are consistent with the energies expected for $M1$ transitions of a rotational band structure built on an 8^- isomer in this nucleus. The energy difference between the two transitions is also consistent for the rotational band structures built on both the 3^+ band below the 2-qp isomer as well as the band built on the 2015-keV state, exhibiting a common moment of inertia of the deformed core within a few percent. Thus the states at 1409 and 1533 keV can be assigned spin-parities of 9^- and 10^- with reasonable confidence. Building on these assignments, the parallel 606- and 482-keV transitions to the 9^- and 10^- states, respectively, restricts the spin of the 2015-keV state to 9, 10, or 11. The fact that the 606-keV transition is the strongest, and no transition to the 8^- bandhead is observed, eliminates a spin assignment of 9. A possible spin of 11 is also ruled out, as an 11^- assignment would entail an $M1$-$E2$ competition where the 482-keV $M1$ intensity should be significantly stronger than the 606-keV $E2$ from Weisskopf estimates, and an 11^+ assignment would require an even more improbable $E1$-$M2$ competition. In addition, the lowest 11^- from a $\pi^2 3^+$ coupled to a $\nu^2 8^-$ excitation, would lie over 700

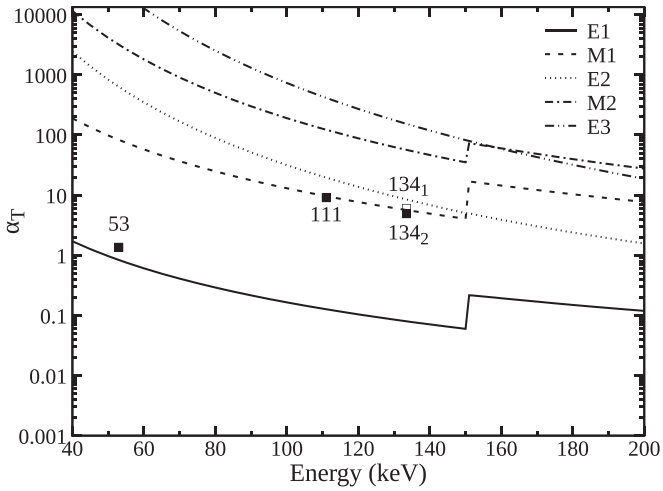

FIG. 6. Total conversion coefficients extracted from intensity balance for selected low-energy transitions in ^{254}No compared with predicted [22] values for different multipolarities. 134_1 and 134_2 denote the $11^+ \rightarrow 10^+$ and $16^+ \rightarrow 15^+$ transitions, respectively.

keV above the observed 10^+ state in our calculations. This leads to a spin assignment of 10 for the intrinsic 2015-keV state. A 10^+ assignment, with both transitions as $E1$, satisfies intensity balance and is the most logical, given that there are no available 10^- configurations from theoretical expectations in this excitation energy range, but a strong candidate for a 10^+ state exists.

The structure built on the 2015-keV state is consistent with the expected energetics of a strongly coupled band of interlocking $M1$ and $E2$ transitions. The intensity balance at each level also bears this out. This leads to a 15^+ assignment for the 2779-keV (rotational) state in this band. Finally, the 2933-keV isomer decays via two parallel transitions to the 14^+ and 15^+ members of this band. The internal conversion coefficient of the 134-keV transition extracted from intensity balance firmly places this as an $M1$ transition (Fig. 6), with the 313-keV parallel transition consistent with an $E2$ assignment. The 4-qp 2933-keV isomer, therefore, is assigned a spin-parity of 16^+ with some confidence, aided by the enhanced statistics and the significant reduction in uncertainties (by a factor of $\approx$2) compared to the earlier study [15]. While all spin-parity assignments should still be considered tentative in the strictest sense since direct multipolarity measurements were not possible, the robust arguments, presented both here and in Ref. [15], provide a strong case for the proposed level scheme.

Two 8^- excited states, one arising from a 2-quasiproton and the other from a 2-quasineutron configuration, are expected in ^{254}No reasonably close in energy and have been the subject of debate regarding the configuration of the established 8^- isomer. No firm evidence of a second 8^- state in the level scheme was found in our present data.

IV. DISCUSSION

A. Configuration Assignments

1. The 3^+ state

Our new measurements for ^{254}No provide a fresh incentive to revisit configuration assignments for 2- and 4-qp states in this nucleus. There is general consensus regarding the structure of the low-lying 3^+ state, which has been assigned a $\pi^2([521]1/2^- \otimes [514]7/2^-)$ configuration [13–16] in prior studies. The intensity ratio of cascade-to-crossover transitions that depopulate members of a rotational band can be used to extract $M1/E2$ branching ratios. The $M1$ component in the $\Delta I = 1$ cascade transition is obtained by subtracting the $E2$ intensity, based on the crossover $E2$ intensity. These ratios can be used to extract experimental $|(g_K - g_R)/Q_0|$ values [23] and compared with theoretical expectations for the intrinsic configuration of the bandhead. Our experimentally deduced $|g_K - g_R|$ value for this band is 0.56(8), using a single branching ratio from an intraband 82-keV ($M1$) and the corresponding 152-keV ($E2$) transition and a Q_0 value of 12.3 eb (with $\approx$10% error) obtained from the 44-keV excitation energy of the 2^+ state in ^{254}No using global systematics [24]. This is in excellent agreement with the theoretical estimate of 0.57 for this configuration, using g_K values of the individual orbitals computed within the WSBETA code [25] with a spin quenching factor of 0.7, and typical values of $g_R = 0.8Z/A$ used for such calculations in this region. This also convincingly rules out a possible $\nu^2([624]7/2^+ \otimes [620]1/2^+)$ assignment [14], which has an expected $|g_K - g_R|$ value of 0.27 [25]. The energy of the $\pi^2 3^+$ configuration is also well reproduced in our calculations [see Fig. 7(a) in Sec. IV C]. This state is especially important since the $\pi[521]1/2^-$ orbital originates from above the next spherical proton shell gap and dips sharply with deformation to become a low-lying valence orbital in ^{254}No, and is the ground state in the next-higher-Z nucleus ^{255}Lr.

2. The 8^- isomer

We now address the configuration of the 8^- isomer, where a firm choice can be made strictly on the basis of excitation energies between three possibilities: (a) $\pi^2([514]7/2^- \otimes [624]9/2^+)$; (b) $\nu^2([734]9/2^- \otimes [613]7/2^+)$; (c) $\nu^2([734]9/2^- \otimes [624]7/2^+)$. In ^{254}No, with $N = 152$, both ν^2 configurations require one or two neutrons from the filled $\nu[734]9/2^-$ level to be promoted across the 1.1–1.2 MeV $N = 152$ shell gap mentioned earlier. In contrast, the π^2 configuration only requires exciting a proton from the $[514]7/2^-$ to the $[624]9/2^+$ orbital, which are both above the $Z = 100$ gap and have a Woods-Saxon (WS) energy separation of $\approx$0.4 MeV. We note that neutron and proton pair gaps for 2-qp excitations are comparable in this region ($\approx$0.5 MeV), as deduced from experimental excitation energies of the low-lying $\pi^2 3^+$ state in ^{254}No (0.988 MeV) and $\nu^2 6^+$ state in ^{244}Cm (1.041 MeV) [26]. The energy difference $(E_{nn} - E_{pp})$ is further increased by GM spin-spin residual interactions. Our calculations, which also includes a 200-keV contribution from spin-spin residual interactions, place the

lower $\nu^2([734]9/2^- \otimes [613]7/2^+)$ state more than 300 keV above the π^2 state [see Fig. 7(a) in Sec. IV C]. Thus, this lowest energy π^2 configuration is strongly favored for the 2-qp 8^- isomer. Mixing of proton and neutron 2-qp states can occur, as in many cases in the Hf region [27] and is discussed later.

In the present work, the rotational band built on the 8^- isomer is not adequately populated to provide an independent experimental argument for the configuration based on extracted $M1/E2$ branching ratios. The argument for a π^2 assignment for the 8^- isomer in earlier work [13,14] also stems from its preferential decay to the rotational band built on the $\pi^2 3^+$ state. The one-body electromagnetic operator, to first order, can only connect states whose wave-functions involve the annihilation of just one particle and the creation of another, and the decay of a $\pi^2 8^-$ isomer to the $\pi^2 3^+$ band is, therefore, allowed because they share a common $[514]7/2^-$ orbital. The $\pi^2 8^-$ assignment differs from Clark *et al.*, who suggested a revised $\nu^2 8^-$ assignment for the isomer based on the fact that the 10^+ state, discussed next, which they first placed and assigned a ν^2 excitation, decays directly to the band built on the 8^- isomer [15].

3. The 10^+ isomer

The lowest intrinsic 10^+ configuration in ^{254}No can only be the $\nu^2([734]9/2^- \otimes [725]11/2^-)$, where the $[734]9/2^-$ state is below the neutron deformed shell gap at $N = 152$ and the $[725]11/2^-$ state above it. Our calculation for the 10^+ excitation energy is within ≈150 keV of the experimental value [see Fig. 7(a) in Sec. IV C]. Note that an upshift of 100 keV was used to account for the GM splitting for this unfavored spin-triplet configuration in our model, but not in the others. In the present work, the average $|g_K - g_R|$ value deduced from the intensity ratios of the cascade-to-crossover transitions depopulating the 13^+, 14^+, and 15^+ members of the rotational band built on this state is 0.42(6). The theoretical $|g_K - g_R|$ estimate for the $\nu^2([734]9/2^- \otimes [725]11/2^-)$ configuration is 0.55. These are in agreement within realistic uncertainties of ≈15%, if we fold in additional experimental uncertainties in gamma-ray efficiencies at low energies, as well as uncertainties in the theoretical estimate.

From considerations of the electromagnetic operator discussed earlier, the decay of the 10^+ state with a $\nu^2([734]9/2^- \otimes [725]11/2^-)$ configuration to the $\pi^2 8^-$ isomer would not be allowed. The simplest manner in which this could be achieved is via a small admixture of the $\nu^2([734]9/2^- \otimes [613]7/2^+)$ 8^- to the $\pi^2 8^-$ wave function, which would provide a common $[734]9/2^-$ neutron orbital between the initial and final states of the decay. As mentioned earlier, mixing of 2-qp neutron and proton are quite common in the $A \approx 180$ region. While the $\nu^2 8^-$ was not directly identified in the present work with the limited statistics, such a state is expected within a few hundred keV above the π^2 state.

4. The 16^+ isomer

Finally, the 4-qp 16^+ isomer can be formed by the $\pi^2 8^-$ configuration coupled with either a $\nu^2([734]9/2^- \otimes [613]7/2^+)$ or a $\nu^2([734]9/2^- \otimes [624]7/2^+)$ 8^- configuration. The former is favored because the latter involves the promotion of two neutrons across the gap as opposed to one [see Fig. 7(a) in Sec. IV C]. While more 4-qp states are predicted in close proximity to the 16^+ in MM calculations, other spin-parity assignments seem to be precluded at this point based on present experimental evidence of its decay pathways. With such a $\pi^2\nu^2$ configuration, the preferential decay of the 4-qp 16^+ isomer to the rotational band built on the 10^+ state, rather than to a band built on the observed 8^- isomer, warrants discussion. Prior to any considerations of the mismatch of K quantum numbers between the initial and final states, the preferential decay of the 16^+ should have been to the rotational band built on the $\pi^2 8^-$ isomer, and not to the $\nu^2 10^+$ band as observed. In the former, only one neutron would have to be paired back, while it is not possible to connect to the $\nu^2 10^+$ via a one-body operator. In this case, the best resolution of this quandary is through a mixing of the 16^+ isomer with the 16^+ member of the rotational band built on the 10^+ state, whose extrapolated energy is only ≈60 keV above it. Some quantitative analysis within this mixing hypothesis provides interesting insights and cross-checks. The experimental transition rate is $\lambda_{\text{expt}} = 1/\tau_{\text{expt}} \approx 3.7 \times 10^3$ s^{-1}. The total transition rate $\lambda_{K=10}$ estimated for a $|I, K\rangle = |16, 10\rangle$ state, using the Q_0 and average $|g_K - g_R|$ values for this band described earlier is 6.5×10^{11} s^{-1}, which is eight orders of magnitude faster than experiment. Thus, if the mixed wave function of the 16^+ isomer is written as $|I, K\rangle = \alpha|16, 16\rangle + \beta|16, 10\rangle$ state, the latter overwhelmingly dominates the transition rate, and $\lambda_{\text{expt}} \approx \beta^2 \lambda_{K=10}$, from which we can extract the admixture $\beta \approx 0.76 \times 10^{-4}$. In the weak-mixing limit, $\beta = V/\Delta E$, where V is the interaction matrix element and ΔE is the energy separation of the two levels. In this case, we extract $V \approx 4$ eV. Even this minuscule mixing provides an unusual pathway in this case for the decay of the 4-qp 16^+ isomer through the 10^+ band members. With the in-band rotational transition rates dominating, the $M1/E2$ branching ratio for the direct 134- and 313-keV decay transitions from the isomer should follow that of the 10^+ band. This is validated within ≈30% error bars, which is not unreasonable if one allows for uncertainties in gamma-ray efficiencies at low energies as well as in determining the intensity sharing in the 134-keV doublet.

This case provides insight on how small admixtures can provide special bypass routes for K-forbidden decays. This is the smallest mixing matrix element observed compared to multiple $\Delta K = 6$ transitions in the $A \approx 180$ region [28–30]. Exploring these small mixing matrix elements between different configurations from a theoretical perspective provides additional insight into the underlying physics [31]. Such accidental K-mixing scenarios between intrinsic 4-qp configurations with rotational excitations built on 2-qp bandheads are expected to occur more frequently in $A \approx 250$ region compared to the $A \approx 180$ region, given the larger density of rotational band levels built on high-K configurations in this heavier region. In the $A \approx 180$ region, 4-qp bandheads lie safely below the most yrast of high-K 2-qp bands, with low-K 2-qp bands lying even higher. The difference is due to two factors: (a) the $A \approx 250$ region has more low-lying high-K

TABLE III. Excitation energies (E_x), spin-parity assignments (K^π) and measured half-lives ($T_{1/2}$) for K isomers in ^{254}No, along with decay transition energies (E_γ), multipolarities, partial γ-ray half-lives ($T^\gamma_{1/2}$), corresponding Weisskopf estimates ($T^W_{1/2}$), degree of K-forbiddenness (ν) and calculated reduced hindrance factors f.

E_x(keV)	K^π	$T_{1/2}$	E_γ(keV)	Mult.	$T^\gamma_{1/2}$(s)	$T^W_{1/2}$(s)	ν	f_ν[a]	f_0[b]
1297	8^-	259(7) ms	53	$E1$	$5.1(2)\times10^{-1}$	1.1×10^{-12}	4	825(6)	$4.6^{+23}_{-14}\times10^{1}$
			778	$E1$	3.3(3)	3.6×10^{-16}	7	191(3)	$3.7^{+9}_{-7}\times10^{1}$
2015	(10^+)	5(2) ns	606	$E1$	$5(2)\times10^{-9}$	7.5×10^{-16}	1	$7(3)\times10^{6}$	$7.0^{+280}_{-55}\times10^{1}$
			482	$E1$	$1.3(6)\times10^{-7}$	1.5×10^{-15}	1	$9(4)\times10^{7}$	$8.6^{+340}_{-68}\times10^{2}$
2933	(16^+)	186(9) µs	134	$M1$	$1.3(2)\times10^{-3}$	9.3×10^{-12}	5	43(1)	9.6^{+4}_{-24}
			313	$E2$	$4.2(6)\times10^{-3}$	1.97×10^{-9}	4	38(2)	$1.2^{+3}_{-2}\times10^{1}$

[a]Extracted using usual prescription $f_\nu = F^{1/\nu}$.
[b]Extracted using prescription in Ref. [33] (see text). F_0 values used: $1.0^{+37}_{-8}\times10^{5}$ ($E1$); $1.7^{+55}_{-3}\times10^{3}$ ($M1$); $1.2^{+17}_{-7}\times10^{2}$ ($E2$). The error bars in f_0 essentially reflect the large uncertainties in F_0 quoted in the compilation fits.

configurations, and (b) the higher rotational inertia for the heavier region leads to a compression of the γ-ray energies. This could lead to complex decays which otherwise would be strictly forbidden and may explain why 4-qp decays may not always follow expected decay routes in the nobelium region.

B. Hindrance factors

While the above discussion identifies specific wave-function admixtures that could provide the transition pathways, we also analyze the K-isomer decays within the formalism developed from compiled systematics of K-hindered transitions. The decay properties of all three isomers are presented in Tables III, where the new half-life of the 2-qp 10^+ isomer extends the available information in this nucleus and this region. The hindrance factor, F, for a K-hindered transition is defined as $(T^{\rm expt}_{1/2}/T^W_{1/2})$, the ratio of the experimental partial half-life to the Weisskopf estimate. Early compilations of F showed an increase by a factor of about 100 per degree of K-forbiddenness, ν, defined as $\Delta K - \lambda$, where λ is the transition multipolarity [32]. Comparisons of K-hindered transitions with varied ΔK and λ, therefore, use $f_\nu = F^{1/\nu}$, the hindrance factor per degree of K-forbiddenness (or reduced hindrance). The 2-qp 8^- and 10^+ isomers decay by two $E1$ transitions each. To avoid arbitrary factors of 10^4 typically used to compare K-hindrances for $E1$ transitions with other multipolarities, a prescription was proposed in Ref. [33] to express the overall hindrance as a product of an underlying intrinsic (or configurational) hindrance F_0 and the additional hindrance f_0 due to K-forbiddenness. This was achieved by fitting the observed dependence of F on ν for different transition multipolarities, with the parametrization $F = F_0 \times f_0^\nu$, which translates to a linear $\log F = \log F_0 + \nu \log f_0$ relationship. Table III includes f_ν values extracted using the standard prescription as well as f_0 values extracted using the new prescription separating K-hindrance from additional configurational hindrance, where the $E1$ hindrances are now more in line with other multipolarities. For $E1$ decays, a fit to the global data yields a K-independent hindrance F_0 of 1.2×10^5, and a K-dependent reduced hindrance f_0 of 12.5, albeit with large uncertainties. These numbers suggest that for $\nu > 4$ in $E1$ decays, K-hindrance dominates, while configuration hindrance dominates at the lowest values of ν. Similar arguments suggest K-hindrance dominating for $M1$ and $E2$ decays with $\nu > 3$ and $\nu > 2$, respectively. In this scenario, the measured half-life and a 2-neutron assignment for the 10^+ state decaying via $\nu = 1$ transitions to a predominantly 2-proton 8^- isomer band would signal a dominance of configurational hindrance over K-hindrance. While not much data is available to compare hindrances and half-lives for K-isomers with different 2-qp configurations connected by low-ν $E1$ decays, examples do exist in the K-isomer-rich $A \approx 180$ region. In ^{180}Hf, for example, a 2-neutron 10^+ decays via three parallel $\nu = 1$ $E1$ transitions to a band built on a 2-proton configuration, where the half-life is below 2 ns [34]. For the decay of the 4-qp 16^+ isomer, a $\Delta K = 6$ pathway (to the 10^+ band) over a $\Delta K = 8$ pathway (to the 8^- band) would be the preferred choice for the 4-qp isomer decay, in spite of any other configuration mismatches, since K hindrance is expected to dominate for large ΔK. Reduced hindrances calculated for the transitions decaying from the 16^+ isomer are 43(2) for the 134-keV $M1$ and 38(2) for the 313-keV $E2$ transition, which are typical values for "good" K isomers.

C. Comparison with theories

The experimental results for the energy levels of key intrinsic excitations (3^+, 8^-, 10^+, 16^+) are first compared to calculations (Fig. 7) to provide a snapshot of the various models in play. The number of different theoretical approaches over the years in calculating detailed level energies for ^{254}No underscores its importance and interest as a touchstone for the structure of superheavy nuclei. Figure 7 a shows our own updated calculations from the model used in Ref. [13], and the same prescription described there. The single-particle energies are obtained from "universal" parameters of the Woods-Saxon (WS) potential [6,25], with $\beta_2 = 0.251$, $\beta_4 = 0.015$, and $\beta_6 = -0.040$, obtained by minimizing the mass with respect to these shape parameters [38], and the Lipkin-Nogami formalism utilized for reduced pairing due to blocking [39]. The strengths of the neutron and proton pairing force ($G_n = 18.5/A$, $G_p = 24.5/A$) are chosen to get agreement between the calculated ground-state pair gaps and the three-point ground-state mass difference for nuclei

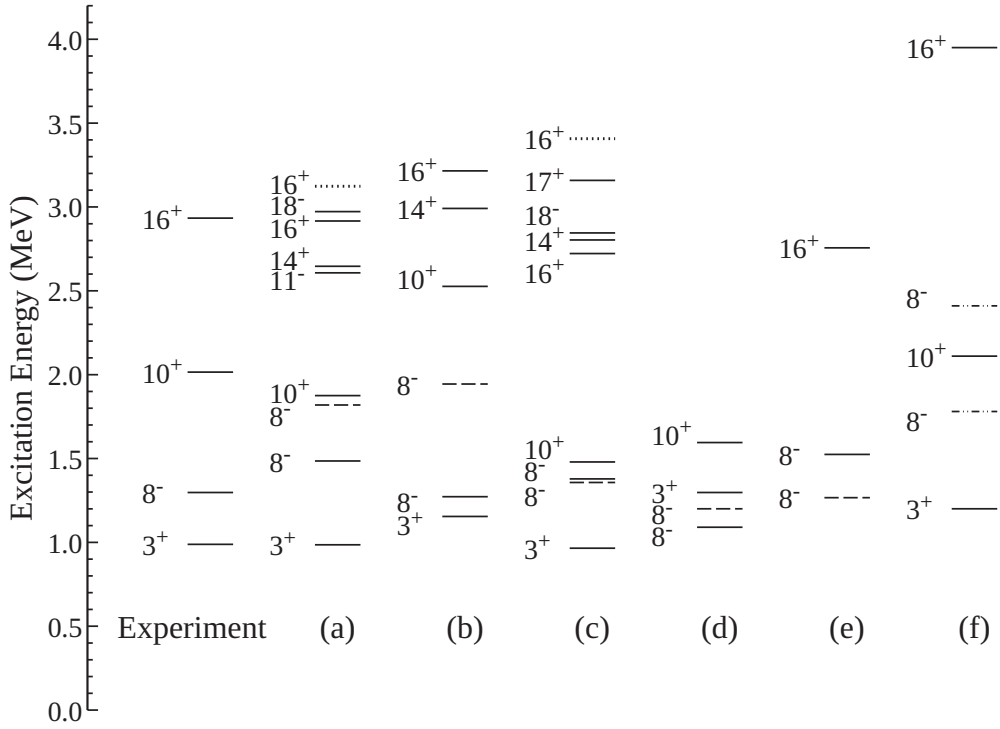

FIG. 7. Experimental excitation energies of intrinsic states in ^{254}No compared with various model calculations (see text): (a) present work; (b) He *et al.* [35]; (c) Liu *et al.* [8,9]; (d) Ivanova *et al.* [36]; (e) Herzberg *et al.* [14]; (f) Robledo *et al.* [37]. For 8^- states, solid (dashed) lines represent the most favored proton (neutron) configurations, respectively, for all except (f), where the 8^- configurations are not specified (see text). For 16^+ states, two configurations are shown, with the π^2 8^- coupled with two possible ν^2 8^- configurations, the ([734]9/2$^-$ ⊗ [613]7/2$^+$) (solid line) and the ([734]9/2$^-$ ⊗ [624]7/2$^+$) (dotted line).

neighboring ^{254}No [40]. The 2-qp states include Gallagher-Moszkowski (GM) spin-spin residual interactions [41,42] of +100 (−100) keV for triplet (singlet) configurations, respectively. For the 4-qp states shown, experimental π^2 values are used and an additional 200 keV is subtracted to account for additional proton-neutron residual interactions. Figure 7(b) is a recent cranked Nilsson calculation that treats pairing correlations using the particle number conservation [35]. Figure 7(c) shows other calculations along our own formalism, with additional configuration constraints [8,9]. Figure 7(d) is one of the earliest calculations performed years before any experimental data in this region, using a semimicroscopic approach that calculated nonrotational 2-qp states beyond actinides from WS single-particle energies [36]. Figure 7(e) is from a projected shell-model approach presented earlier in Ref. [14]. The most recent calculations for 2-qp and 4-qp excitations come from a self-consistent Hartree-Fock-Bogoliubov method using a density-dependent finite range Gogny force parametrization including full blocking [Fig. 7(f)] [37]. Note that the residual interactions are included in the model of Fig. 7(a) and in Fig. 7(e) calculated by the projected shell model (see Ref. [43]), but are not included in other figures.

In each of these theories, the calculated SPEs provide a crucial check against experiment. When the SPE spectrum exhibits a gap, excited states where a quasiparticle is promoted across the gap have larger energies that scale with the gap size—a clear signature we employ for configuration assignments. The MM models (a), (b), and (c) use neutron SPEs with $N = 152$ gaps of 1.1–1.2 MeV in fermium and nobelium, which increase when the correct shape with high-order deformation, especially β_6, is included to minimize the mass [5,7]. In (a) and (b), the 2-qp states where one quasiparticle is excited across the unambiguously established $N = 152$ gap [44,45] have high excitation energy. In (c), neither the $\nu^2 8^-$ nor the $\nu^2 10^+$ are raised to the expected extent, presenting an unexplained problem. These energies are also not elevated in (d), but here the reason is clear: these calculations were performed before the importance of high-order deformation was established, and, therefore, were not included. The SPEs employed in the projected shell model calculation in (e) were not provided. In (f), the calculated 2-qp energies are explained by their SPEs, with a reduced $N = 152$ gap and a very high energy for the π[624]9/2+ orbital, resulting in a lower $\nu^2 8^-$ compared to the $\pi^2 8^-$.

Two-qp states provide a compact way to compare models via the energies and predictions for the state that constitutes the isomer. High-K states offer a particularly sensitive probe of high-j orbitals. Energies of both $K = 3^+$ and 8^-, which involve proton configurations, as well as the $K = 10^+$ and $K = 16^+$, which involve neutron configurations, are well described with the use of the WS potential. In contrast, density functional theories with the SLy4 and D1S functionals give a fair description of the $K = 3^+$ state [11,37], but yield 8^- energies which are excessively high. Furthermore, the lowest-energy high-K state, which should constitute the K-isomer, has the wrong configuration with $K = 7^-$ [11]. A quick

inspection of the SPE spectra reveals that the high-j orbitals lie too high. As a result, instead of known gaps at $Z = 100$ and $N = 152$, which are reproduced by WS SPE, the density functionals generally yield proton gaps at the wrong positions ($Z = 98$ and 104) and a degeneracy at $Z = 100$, and diminished neutron gaps at N = 150 and 152, instead of one large gap at $N = 152$ [46]. In order to correct the high-j energies, local tuning of spin-orbit constants to lower the energies of intruder shells has yielded good effect, although the $N = 152$ gap remains underestimated [47]. An extension of this interesting exercise to a broader span of nuclei may lead to an improved functional. While new theoretical approaches and fresh perspectives are being continually added to the mix [48], each will have to be tested against the same benchmarks. The obvious success of WS potentials in describing experimental data in ^{254}No provides confidence in extrapolating their reach to describe superheavy nuclei.

Parallel experimental efforts in prompt spectroscopy will also be needed for a comprehensive understanding of the isomeric configurations in ^{254}No through their respective rotational band structures. There is ongoing analysis with a data set collected for ^{254}No with the Gammasphere array tagged by evaporation recoils in AGFA [49] to investigate prompt feeding of the bands built on the 8^- and 16^+ isomers. Significantly higher γ-γ coincidence statistics are required, however, for definitive and unbiased experimental level schemes, which may be attempted with next-generation high-efficiency gamma-ray arrays nearing completion. Deviations from simple axial quadrupole shapes in ^{254}No and neighboring nuclei are also an active area of theoretical research (see Ref. [50] and references therein) that have a bearing on the goodness of the K quantum number. This gateway nucleus will undoubtedly continue to be a critical testing ground for superheavy theories.

V. CONCLUSION

In summary, a new decay-spectroscopy study of high-K isomers in ^{254}No, using the gas-filled analyzer AGFA at Argonne National Laboratory, resolves long-standing ambiguities and establishes a more confident level scheme and spin-parity assignments with the highest γ-γ coincidence statistics to date. A new isomeric short half-life is identified and measured in this nucleus to establish a second 2-qp isomer in ^{254}No. Firm assignments are made for the two lowest 2-qp states as proton configurations, resolving previous controversies regarding the 8^- isomer. With configuration ambiguities removed, the intrinsic excitations in this deformed mass region provide stringent constraints and challenge the different theoretical approaches (e.g. macroscopic-microscopic versus density functional) which attempt to understand the structure of superheavy nuclei. Using information on 2-qp high-K isomers, we suggest that the problem lies in the high-j orbitals being too high in energy in the current best functionals.

ACKNOWLEDGMENTS

We thank the entire ANL accelerator and scientific staff for setting up the infrastructure to run this experiment in remote mode during the COVID shutdown, and Dr. S.K. Tandel for helpful discussions during the preparation of the manuscript. This material is based upon work supported by the US Department of Energy, Office of Science, Office of Nuclear Physics, under Grant No. DE-FG02-94ER40848(UML) and Contracts No. DE-AC02-06CH11357 (ANL), No. DE-AC02-05CH11231 (LBNL), and No. DE-AC02-98CH10946 (BNL). This research used resources of ANL's ATLAS facility, which is a DOE Office of Science User Facility. Support from the Science and Technology Facilities Council (UK) is acknowledged.

[1] R.-D. Herzberg and P. T. Greenlees, Prog. Part. Nucl. Phys. **61**, 674 (2008).
[2] C. Theisen, P. T. Greenlees, T. L. Khoo, P. Chowdhury, and T. Ishii, Nucl. Phys. A **944**, 333 (2015).
[3] P. Reiter, T. L. Khoo, C. J. Lister, D. Seweryniak, I. Ahmad, M. Alcorta, M. P. Carpenter, J. A. Cizewski, C. N. Davids, G. Gervais, J. P. Greene, W. F. Henning, R. V. F. Janssens, T. Lauritsen, S. Siem, A. A. Sonzogni, D. Sullivan, J. Uusitalo, I. Wiedenhöver, N. Amzal, P. A. Butler, A. J. Chewter, K. Y. Ding, N. Fotiades, J. D. Fox, P. T. Greenlees, R.-D. Herzberg, G. D. Jones, W. Korten, M. Leino, and K. Vetter, Phys. Rev. Lett. **82**, 509 (1999).
[4] Y. Oganessian, J. Phys. G: Nucl. Part. Phys. **34**, R165 (2007).
[5] A. Sobiczewski, I. Muntian, and Z. Patyk, Phys. Rev. C **63**, 034306 (2001).
[6] S. Ćwiok, S. Hofmann, and W. Nazarewicz, Nucl. Phys. A **573**, 356 (1994).
[7] A. Sobiczewski and K. Pomorski, Prog. Part. Nucl. Phys. **58**, 292 (2007).
[8] H. L. Liu, F. R. Xu, P. M. Walker, and C. A. Bertulani, Phys. Rev. C **83**, 011303(R) (2011).
[9] H. L. Liu, P. M. Walker, and F. R. Xu, Phys. Rev. C **89**, 044304 (2014).
[10] A. V. Afanasjev, T. L. Khoo, S. Frauendorf, G. A. Lalazissis, and I. Ahmad, Phys. Rev. C **67**, 024309 (2003).
[11] J. P. Delaroche, M. Girod, H. Goutte, and J. Libert, Nucl. Phys. A **771**, 103 (2006).
[12] T. Duguet, P. Bonche, and P. H. Heenen, Nucl. Phys. A **679**, 427 (2001).
[13] S. K. Tandel, T. L. Khoo, D. Seweryniak, G. Mukherjee, I. Ahmad, B. Back, R. Blinstrup, M. P. Carpenter, J. Chapman, P. Chowdhury, C. N. Davids, A. A. Hecht, A. Heinz, P. Ikin, R. V. F. Janssens, F. G. Kondev, T. Lauritsen, C. J. Lister, E. F. Moore, D. Peterson, P. Reiter, U. S. Tandel, X. Wang, and S. Zhu, Phys. Rev. Lett. **97**, 082502 (2006).
[14] R.-D. Herzberg, P. T. Greenlees, P. A. Butler, G. D. Jones, M. Venhart, I. G. Darby, S. Eeckhaudt, K. Eskola, T. Grahn, C. Gray-Jones, F. P. Hessberger, P. Jones, R. Julin, S. Juutinen, S. Ketelhut, W. Korten, M. Leino, A.-P. Leppänen, S. Moon, M. Nyman, R. D. Page, J. Pakarinen, A. Pritchard, P. Rahkila, J. Sarén, C. Scholey, A. Steer, Y. Sun, C. Theisen, and J. Uusitalo, Nature (London) **442**, 896 (2006).
[15] R. M. Clark, K. E. Gregorich, J. S. Berryman, M. N. Ali, J. M. Allmond, C. W. Beausang, M. Cromaz, M. A. Deleplanque, I. Dragojević, J. Dvorak, P. A. Ellison, P. Fallon, M. A. Garcia, J. M. Gates, S. Gros, H. B. Jeppesen, D. Kaji, I. Y. Lee, A. O.

Macchiavelli, K. Morimoto, H. Nitsche, S. Paschalis, M. Petri, L. Stavsetra, F. S. Stephens, H. Watanabe, and M. Wiedeking, Phys. Lett. B **690**, 19 (2010).
[16] F. P. Heßberger, S. Antalic, B. Sulignano, D. Ackermann, S. Heinz, S. Hofmann, B. Kindler, J. Khuyagbaatar, I. Kojouharov, P. Kuusiniemi, M. Leino, B. Lommel, R. Mann, K. Nishio, A. G. Popeko, S. Sáro, B. Streicher, J. Uusitalo, M. Venhart, and A. V. Yeremin, Eur. Phys. J. A **43**, 55 (2010).
[17] A. J. Mitchell, P. F. Bertone, B. DiGiovine, C. J. Lister, M. P. Carpenter, P. Chowdhury, J. A. Clark, N. DOlympia, A. Y. Deo, F. G. Kondev, E. A. McCutchan, J. Rohrer, G. Savard, D. Seweryniak, and S. Zhu, Nucl. Instrum. Methods Phys. Res., Sect. A **763**, 232 (2014).
[18] R. Brun and F. Rademakers, Nucl. Instrum. Methods Phys. Res., Sect. A **389**, 81 (1997).
[19] D. C. Radford, Nucl. Instrum. Methods Phys. Res., Sect. A **361**, 297 (1995).
[20] C. Gray-Jones, Ph.D. thesis, University of Liverpool, 2008.
[21] R.-D. Herzberg (private communication).
[22] T. Kibédi, T. W. Burrows, M. B. Trzhaskovskaya, P. M. Davidson, and C. W. Nestor Jr., Nucl. Instrum. Methods Phys. Res., Sect. A **589**, 202 (2008).
[23] P. Alexander, F. Boehm, and E. Kankeleit, Phys. Rev. **133**, B284 (1964).
[24] S. Raman, C. Nestor, and P. Tikkanen, At. Data Nucl. Data Tables **78**, 1 (2001).
[25] S. Cwiok, J. Dudek, W. Nazarewicz, J. Skalski, and T. Werner, Comput. Phys. Commun. **46**, 379 (1987).
[26] S. E. Vandenbosch and P. Day, Nucl. Phys. **30**, 177 (1962).
[27] T. L. Khoo, J. C. Waddington, R. A. O'Neil, Z. Preibisz, D. G. Burke, and M. W. Johns, Phys. Rev. Lett. **28**, 1717 (1972).
[28] G. D. Dracoulis, F. G. Kondev, G. J. Lane, A. P. Byrne, T. R. McGoram, T. Kibédi, I. Ahmad, M. P. Carpenter, R. V. F. Janssens, T. Lauritsen, C. J. Lister, D. Seweryniak, P. Chowdhury, and S. K. Tandel, Phys. Rev. Lett. **97**, 122501 (2006).
[29] T. R. Saitoh, N. Saitoh-Hashimoto, G. Sletten, R. A. Bark, G. B. Hagemann, and B. Herskind, Phys. Scr. **T88**, 67 (2000).
[30] P. M. Walker, R. J. Wood, G. D. Dracoulis, T. Kibédi, R. A. Bark, A. M. Bruce, A. P. Byrne, P. M. Davidson, H. M. El-Masri, G. J. Lane, C. Moon, J. N. Orce, F. M. P. Estevéz, C. Wheldon, and A. N. Wilson, Phys. Rev. C **79**, 044321 (2009).
[31] F.-Q. Chen, Y.-X. Liu, Y. Sun, P. M. Walker, and G. D. Dracoulis, Phys. Rev. C **85**, 024324 (2012).
[32] K. E. G. Löbner, Phys. Lett. B **26**, 369 (1968).
[33] F. G. Kondev, G. D. Dracoulis, and T. Kibédi, At. Data Nucl. Data Tables **103-104**, 50 (2015).
[34] S. K. Tandel, P. Chowdhury, F. G. Kondev, R. V. F. Janssens, T. L. Khoo, M. P. Carpenter, T. Lauritsen, C. J. Lister, D. Seweryniak, S. Zhu, A. Deacon, S. J. Freeman, N. J. Hammond, G. D. Jones, E. F. Moore, and J. F. Smith, Phys. Rev. C **94**, 064304 (2016).
[35] X.-T. He, S.-Y. Zhao, Z.-H. Zhang, and Z.-Z. Ren, Chin. Phys. C **44**, 034106 (2020).
[36] S. P. Ivanova, A. L. Komov, L. A. Malov, and V. G. Soloviev, Sov. J. Part. Nucl. **7**, 175 (1976).
[37] L. M. Robledo, J. Phys. G: Nucl. Part. Phys. **51**, 045108 (2024).
[38] P. Möller, A. Sierk, T. Ichikawa, and H. Sagawa, At. Data Nucl. Data Tables **109-110**, 1 (2016).
[39] Y. Nogami, Phys. Rev. **134**, B313 (1964).
[40] W. Huang, M. Wang, F. Kondev, G. Audi, and S. Naimi, Chin. Phys. C **45**, 030002 (2021).
[41] C. J. Gallagher and S. A. Moszkowski, Phys. Rev. **111**, 1282 (1958).
[42] C. J. Gallagher, Phys. Rev. **126**, 1525 (1962).
[43] Y. Sun, Phys. Scr. **91**, 043005 (2016).
[44] J. Qian, A. Heinz, T. L. Khoo, R. V. F. Janssens, D. Peterson, D. Seweryniak, I. Ahmad, M. Asai, B. B. Back, M. P. Carpenter, A. B. Garnsworthy, J. P. Greene, A. A. Hecht, C. L. Jiang, F. G. Kondev, T. Lauritsen, C. J. Lister, A. Robinson, G. Savard, R. Scott, R. Vondrasek, X. Wang, R. Winkler, and S. Zhu, Phys. Rev. C **79**, 064319 (2009).
[45] M. Asai, K. Tsukada, H. Haba, Y. Ishii, T. Ichikawa, A. Toyoshima, T. Ishii, Y. Nagame, I. Nishinaka, Y. Kojima, and K. Sueki, Phys. Rev. C **83**, 014315 (2011).
[46] J. Dobaczewski, A. V. Afanasjev, M. Bender, L. M. Robledo, and Y. Shi, Nucl. Phys. A **944**, 388 (2015), special Issue on Superheavy Elements.
[47] Y. Shi, J. Dobaczewski, and P. T. Greenlees, Phys. Rev. C **89**, 034309 (2014).
[48] D. D. Dao and F. Nowacki, Phys. Rev. C **105**, 054314 (2022).
[49] C. Morse and T. Huang (private communication).
[50] F. F. Xu, Y. K. Wang, Y. P. Wang, P. Ring, and P. W. Zhao, Phys. Rev. Lett. **133**, 022501 (2024).